

# Two-dimensional Holstein-Hubbard model: Critical temperature, Ising universality, and bipolaron liquid

Manuel Weber and Martin Hohenadler

*Institut für Theoretische Physik und Astrophysik, Universität Würzburg, 97074 Würzburg, Germany*

(Dated: August 6, 2018)

The two-dimensional Holstein-Hubbard model is studied by means of continuous-time quantum Monte Carlo simulations. Using renormalization-group-invariant correlation ratios and finite-size extrapolation, the critical temperature of the charge-density-wave transition is determined as a function of coupling strength, phonon frequency, and Hubbard repulsion. The phase transition is demonstrated to be in the universality class of the two-dimensional Ising model and detectable via the fidelity susceptibility. The structure of the ground-state phase diagram and the possibility of a bipolaronic metal with a single-particle gap above  $T_c$  are explored.

## I. INTRODUCTION

Phase transitions in two-dimensional (2D) fermionic systems are a central topic of theoretical and experimental condensed matter physics. Correlated quasi-2D materials with rich phase diagrams include high-temperature superconductors [1] and transition-metal dichalcogenides [2]. Dirac fermions in two dimensions can be investigated in graphene [3]. Strongly correlated 2D fermions exhibit exotic phases [4] and phase transitions [5], and can support long-range order at  $T > 0$  [6]. While magnetism originates from short-range Coulomb repulsion, the main mechanism behind the numerous charge-density-wave (CDW) phases found experimentally is electron-phonon coupling. In addition to polaron effects, the latter leads to a phonon-mediated, retarded electron-electron interaction and an intricate interplay of spin, charge, and lattice fluctuations.

Quantum Monte Carlo (QMC) simulations are a key tool to investigate correlated 2D quantum systems. Although simulations are significantly harder for fermions than for spins or bosons, QMC methods have been very successfully applied to fermionic models. However, whereas the phase diagram and critical behavior of, e.g., the 2D honeycomb Hubbard model is known in detail [7–10], the same is not true even for the simplest Holstein molecular-crystal model of electron-phonon interaction. Most notably, simulations with phonons are often severely restricted by long autocorrelation times also away from critical points [11]. Currently, reliable critical temperatures, convincing analysis of critical behavior, and the ground-state phase diagram remain key open problems. In fact, even the simpler 1D case had until recently been discussed controversially [12], with earlier claims of dominant pairing correlations refuted by direct calculations of the correlation functions and traced back to spin gap formation [13].

Here, we use large-scale continuous-time QMC simulations to investigate the CDW transition in the 2D Holstein-Hubbard model. Although the latter has been extensively studied in the past, important open questions remain. At strong coupling and half-filling, the ground state is either a CDW insulator or an antiferromagnetic

Mott insulator. Recent variational QMC studies [14, 15] argue in favor of a third phase (metallic or superconducting), seemingly in contradiction with theoretical arguments based on weak-coupling instabilities of the Fermi liquid [16, 17]. We use finite-size scaling to determine  $T_c$  of the CDW transition, show that the latter can also be detected by the fidelity susceptibility, and provide evidence for its Ising critical behavior. Moreover, we present arguments and data for the existence of a metallic bipolaron phase at  $T > T_c$  and address the possibility of a metallic or a superconducting ground state.

The paper is organized as follows. Section II introduces the relevant models, Sec. III gives a brief review of the numerical methods, Sec. IV discusses the results, and Sec. V contains our conclusions.

## II. MODELS

The Holstein-Hubbard Hamiltonian [18] reads

$$\hat{H} = -t \sum_{\langle i,j \rangle \sigma} \hat{c}_{i\sigma}^\dagger \hat{c}_{j\sigma} + \sum_i \left[ \frac{1}{2M} \hat{P}_i^2 + \frac{K}{2} \hat{Q}_i^2 \right] - g \sum_i \hat{Q}_i \hat{\rho}_i + U \sum_i (\hat{n}_{i\uparrow} - \frac{1}{2})(\hat{n}_{i\downarrow} - \frac{1}{2}). \quad (1)$$

The first two terms describe free electrons and free phonons, respectively. Here,  $\hat{c}_{i\sigma}^\dagger$  creates an electron with spin  $\sigma$  at lattice site  $i$  and electrons hop with amplitude  $t$  between nearest-neighbor sites on a square lattice. The phonons are of the Einstein type with frequency  $\omega_0 = \sqrt{K/M}$ ; their displacements  $\hat{Q}_i$  couple to local fluctuations  $\hat{\rho}_i = \hat{n}_i - 1$  of the electron occupation  $\hat{n}_i = \sum_\sigma \hat{n}_{i\sigma}$  where  $\hat{n}_{i\sigma} = \hat{c}_{i\sigma}^\dagger \hat{c}_{i\sigma}$ . The last term describes a Hubbard onsite repulsion of strength  $U$ . We simulated  $L \times L$  lattices with periodic boundary conditions at half-filling ( $\langle \hat{n}_i \rangle = 1$ , chemical potential  $\mu = 0$ ). A useful dimensionless coupling parameter is  $\lambda = g^2/(WK)$  with the free bandwidth  $W = 8t$ . We set  $\hbar$ ,  $k_B$ , and the lattice constant to one and use  $t$  as the energy unit.

For  $U = 0$ , Eq. (1) reduces to the Holstein model. Its relative simplicity has motivated numerous QMC investigations of CDW formation and superconductivity

[17, 19–26]. Equation (1) with  $g = 0$  corresponds to the repulsive Hubbard model on the square lattice. At half-filling, the ground state of the latter is an antiferromagnetic Mott insulator for any  $U > 0$  [27]. However, in contrast to CDW order, antiferromagnetism is restricted to  $T = 0$  in two dimensions by the Mermin-Wagner theorem [6]. The full Holstein-Hubbard Hamiltonian (1) captures the competition between Mott and CDW ground states [14, 28–33]. Whereas early work unanimously agreed on the absence of a disordered or a superconducting ground state at half-filling, such a phase has recently been advocated by numerical results [14, 15].

Because it is sufficient to address many of the open questions of interest, we will mainly consider the case  $U = 0$ . However, selected results for the impact of the Hubbard repulsion will also be reported. For Eq. (1) with  $U = 0$ , mean-field theory (exact for  $\omega_0 = 0$  and  $T = 0$ ) predicts a CDW ground state with a checkerboard pattern for the lattice displacements and the charge density [ordering vector  $\mathbf{Q} = (\pi, \pi)$ , see inset of Fig. 1] at half-filling [17, 19, 21]. Here, we systematically explore the impact of quantum and thermal fluctuations.

An important limiting case is the antiadiabatic limit  $\omega_0 \rightarrow \infty$ , in which the Holstein-Hubbard model maps to a Hubbard model with Hamiltonian

$$\hat{H} = -t \sum_{\langle i,j \rangle \sigma} \hat{c}_{i\sigma}^\dagger \hat{c}_{j\sigma} + U_\infty \sum_i (\hat{n}_{i\uparrow} - \frac{1}{2})(\hat{n}_{i\downarrow} - \frac{1}{2}) \quad (2)$$

and effective interaction  $U_\infty = U - \lambda W$ . For  $U = 0$ , interactions are purely attractive and give rise to coexisting CDW and superconducting order for any  $\lambda > 0$  at  $T = 0$ . However, at half-filling, this order is minimal in the sense that  $T_c = 0$  [34], which is related to a perfect degeneracy of CDW and pairing correlations and an associated continuous  $SO(3)$  order parameter for which the Mermin-Wagner theorem applies [6].

### III. METHODS

Extending previous applications to 1D electron-phonon models [35–37], we use the continuous-time interaction expansion (CT-INT) method [38]. To this end, we express the partition function as a functional integral

$$Z = \int \mathcal{D}(\bar{c}, c) e^{-S_0[\bar{c}, c]} e^{-S_1[\bar{c}, c]} \int \mathcal{D}(\bar{b}, b) e^{-S_{\text{ep}}[\bar{c}, c, \bar{b}, b]} \quad (3)$$

using coherent states. Splitting the action into the free-fermion part  $S_0$ , the Hubbard interaction  $S_1$ , and the remainder  $S_{\text{ep}}$  that contains the free-phonon contribution and the electron-phonon coupling, the phonons are integrated out analytically to arrive at a fermionic model with both an instantaneous Hubbard interaction ( $S_1$ ) and a retarded, phonon-mediated interaction ( $S_2$ ) [39]. This model can be simulated by the CT-INT method by sampling both types of vertices [39] to stochastically sum

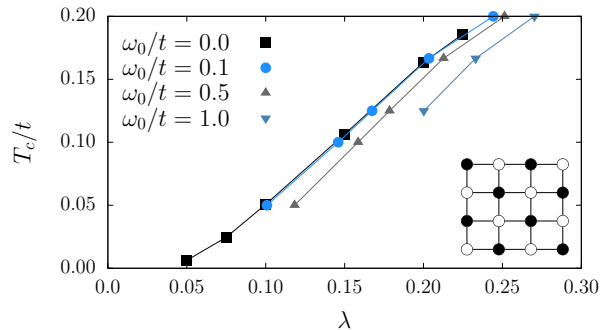


FIG. 1. Critical temperature of the Holstein model ( $U = 0$ ) from finite-size scaling. Here and in subsequent figures, lines are guides to the eye. Statistical errors are smaller than the symbols, see text. The inset illustrates the CDW order at  $T < T_c$  for  $L = 4$ , with filled (open) symbols representing occupied (empty) sites.

the weak-coupling Dyson expansion [38] around  $S_0$ . Because the latter converges for fermionic systems in a finite spacetime volume, CT-INT is exact apart from statistical errors. Technical reviews can be found in Refs. [40, 41].

In contrast to the determinant QMC (DetQMC) method [42] used in almost all previous works on Holstein-Hubbard-type models, CT-INT has significantly smaller autocorrelation times [11]. CT-INT simulation times scale as  $O(n^3)$ , where  $n \approx O(\lambda\beta L^2)$  for  $U = 0$  is the average expansion order and  $\beta = 1/T$ . Although DetQMC formally has a better  $O(\beta L^6)$  scaling, CT-INT benefits from reduced expansion orders at weak coupling and seems to outperform DetQMC for most parameters considered despite being limited for  $\omega_0 \gtrsim t$  by a sign problem. Whereas even the noninteracting case is challenging for DetQMC, CT-INT trivially gives exact results for  $\lambda = 0$  and can in principle simulate the entire range of phonon frequencies, including the experimentally important adiabatic regime  $\omega_0 < t$ . We used up to 5000 single-vertex updates and 8 Ising spin flips per sweep. The classical case  $\omega_0 = 0$  was simulated using the method of Ref. [43] combined with parallel tempering [44].

### IV. RESULTS

Since the effect of electron-electron repulsion on a half-filled square lattice—namely, an antiferromagnetic Mott state at  $T = 0$ —is well understood [27] the focus of our work will be the electron-phonon interaction, i.e., Eq. (1) with  $U = 0$ . Coulomb interactions of the Hubbard or even long-range type can be simulated with unbiased QMC methods on systems large enough to extract critical exponents [7–10]. In contrast, the electron-phonon interaction is significantly more challenging to describe due to the resulting, retarded electron-electron interaction. This is true both for QMC methods but also for, e.g., the functional renormalization group [30, 31]. Consequently, even

fundamental aspects such as the existence of a nonzero critical value for the CDW transition are still under debate. From the 1D Holstein-Hubbard model, it is known that the phases at  $U = 0$  (Luther-Emery liquid and CDW insulator) are stable against a nonzero Hubbard repulsion so that they and the phase transition between them can be fully understood in the simpler Holstein model [12]. In particular, the metallic phase arises from quantum lattice fluctuations rather than from a competing Hubbard interaction [12]. In the 2D case, recent predictions of an extended metallic region suggest that the latter is largest at  $U = 0$  [14, 15]. A nonzero but sufficiently small Hubbard repulsion merely shifts the critical value for the CDW transition [14, 28–33]. Moreover, because the long-range antiferromagnetic order is restricted to  $T = 0$ , the possible phases at  $T > 0$  (the focus of this work) remain the same.

### A. Critical values

To obtain the critical values shown in Fig. 1, we calculated the correlation ratio [45]

$$R_c = 1 - \frac{S_c(\mathbf{Q} - \delta\mathbf{q})}{S_c(\mathbf{Q})} \quad (4)$$

(with  $|\delta\mathbf{q}| = 2\pi/L$ ) from the charge structure factor

$$S_c(\mathbf{q}) = \frac{1}{L^2} \sum_{ij} e^{i(\mathbf{r}_i - \mathbf{r}_j) \cdot \mathbf{q}} \langle \hat{n}_i \hat{n}_j \rangle \quad (5)$$

either at fixed  $\lambda$  or at fixed  $T$ . Here,  $\mathbf{Q} = (\pi, \pi)$ . By definition, a divergence of  $S_c(\mathbf{Q})$  with  $L$  in the CDW phase implies  $R_c \rightarrow 1$  for  $L \rightarrow \infty$ , whereas  $R_c \rightarrow 0$  in the absence of long-range CDW order. Moreover, because  $R_c$  is a renormalization group invariant [45], the critical point can be estimated from the crossing of curves for different  $L$ , as illustrated in Fig. 2(a) for  $\omega_0/t = 0.1$  and  $T/t = 0.05$ . While the correlation ratio (4) is expected

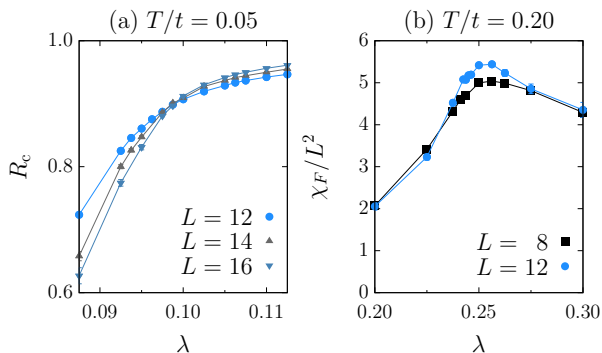


FIG. 2. (a) Determination of the critical value  $\lambda_c$  from (a) the crossing of the correlation ratios  $R_c$  for different system sizes  $L$  and (b) the maximum in the fidelity susceptibility. Here,  $\omega_0/t = 0.1$ ,  $U = 0$ , and (a)  $T/t = 0.05$ , (b)  $T/t = 0.2$ .

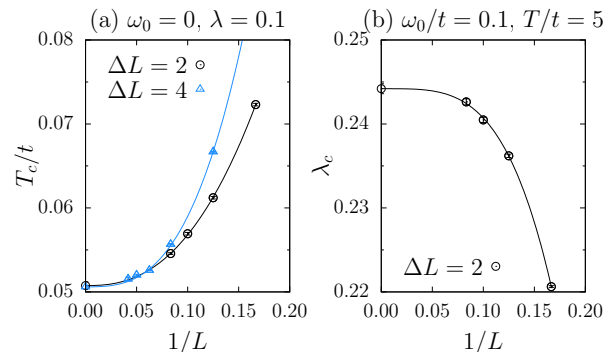


FIG. 3. Finite-size extrapolation of the crossing points of  $R_c(L)$ ,  $R_c(L - \Delta L)$  using the fit function (6). Here, (a)  $\omega_0 = 0$ ,  $\lambda = 0.1$ ,  $T_c = 0.0506(1)$  and (b)  $\omega_0/t = 0.1$ ,  $T/t = 0.2$ ,  $\lambda_c = 0.244(1)$ .

to exhibit smaller finite-size corrections than the structure factor (5), a shift of consecutive crossing points is observed on the accessible system sizes, making it necessary to extrapolate to  $L = \infty$ . To this end, we used a fit function

$$f(L) = a + bL^c. \quad (6)$$

Examples for such extrapolations are shown for  $\omega_0/t = 0$  in Fig. 3(a) and for  $\omega_0/t = 0.1$  in Fig. 3(b). For classical phonons, we can access significantly larger system sizes up to  $L = 28$ . The points in Fig. 3(a) correspond to crossing points of  $R_c$  for  $L$ ,  $L - 2$  (i.e.,  $\Delta L = 2$ ) and  $L$ ,  $L - 4$  ( $\Delta L = 4$ ), respectively. Fitting to Eq. (6), these two choices yield identical results for  $T_c$  within error bars. The errors take into account the statistical errors of the QMC results as well as the errors in determining the crossing points using parabolic fits (obtained from a bootstrap analysis) and extrapolating to  $L = \infty$ . They are smaller than the symbol size in Fig. 1 but naturally do not capture possible variations due to the choice of fit function or observable. For quantum phonons, we systematically used  $L = 4, 6, 8, 10, 12$  and hence  $\Delta L = 2$ , as illustrated in Fig. 3(b). A similar extrapolation gives  $\lambda_c = 0.101(1)$  for the parameters of Fig. 2(a).

The phase transition can also be detected using the fidelity susceptibility  $\chi_F$  [46], an unbiased diagnostic to detect critical points without any knowledge about the order parameter. It essentially relies on calculating the overlap of the ground states of (in the present case) Holstein Hamiltonians with couplings  $\lambda$  and  $\lambda + \delta\lambda$ . A finite-temperature generalization has been given in Refs. [47–49] and CT-INT estimators in Refs. [50, 51]. Although these estimators have rather large statistical errors at low temperatures,  $\chi_F/L^2$  for  $T/t = 0.20$  in Fig. 2(b) shows the expected peak at a position that is consistent with Fig. 1 and  $\lambda_c = 0.244(1)$  from Fig. 3(b).

Figure 1 shows  $T_c(\lambda)$  for different  $\omega_0$ , covering the entire adiabatic regime  $0 \leq \omega_0 \leq t$ . The mean-field result  $T_c \sim e^{-1/\sqrt{\lambda}}$  for the 2D Holstein model—compared to  $T_c \sim e^{-1/\lambda}$  in dynamical mean-field theory (DMFT)

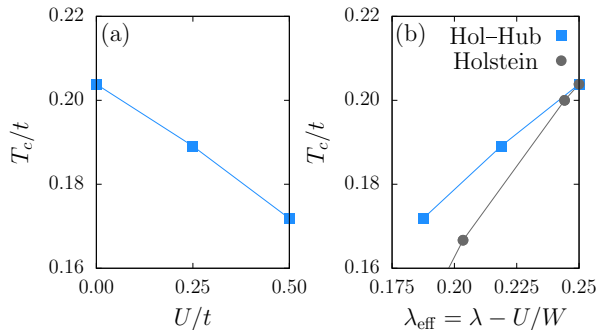


FIG. 4. Critical temperature of the CDW transition in the Holstein-Hubbard model. (a) Suppression of  $T_c$  with increasing  $U$  at  $\lambda = 0.25$  from finite-size scaling, (b) comparison of Holstein and Holstein-Hubbard results in terms of the effective coupling  $\lambda_{\text{eff}} = \lambda - U/W$ . The points labeled ‘Hol-Hub’ correspond to  $\lambda_c$  at different temperatures from Fig. 1. The points labeled ‘Hol-Hub’ (Holstein-Hubbard) are for  $T_c$  at  $\lambda = 0.25$  and  $U/t = 0, 0.25, 0.50$  from (a). Here,  $\omega_0/t = 0.1$ .

[52]—is expected to overestimate  $T_c$  even at  $\omega_0 = 0$  and does not capture the expected maximum at  $\lambda < \infty$  [52]. The latter is outside the range of couplings considered here. Quantum lattice fluctuations suppress  $T_c$  at a given  $\lambda$ . For  $\omega_0/t = 0.1$ ,  $T_c$  shows only minor deviations from the result for classical phonons, whereas for larger  $\omega_0$  quantum fluctuation effects are clearly visible over the entire parameter range shown. The systematic suppression of  $T_c$  with increasing  $\omega_0$  is perfectly consistent with the fact that  $T_c = 0$  for the attractive Hubbard model [34], to which the Holstein model maps in the limit  $\omega_0 \rightarrow \infty$  [53]. This connection and a possible metallic phase at low temperatures as a result of quantum fluctuations will be discussed below. At  $T > 0$ , a metallic region is naturally expected in the phase diagram of the 2D Holstein-Hubbard model because the antiferromagnetic Mott state arising from the Hubbard interaction is confined to  $T = 0$ . In contrast to previous DMFT results [52], the critical temperatures in Fig. 1 were obtained by taking into account all (spatial and temporal) fluctuations on the square lattice.

The Hubbard repulsion suppresses CDW order [14, 28–33]. This is already apparent from the effective Hubbard model (2) in the limit  $\omega_0 \rightarrow \infty$  where a nonzero  $U$  reduces the effective, attractive interaction and thereby the CDW gap at  $T = 0$ . Whereas CDW order is restricted to  $T = 0$  in this limit, here we consider the Holstein-Hubbard model in the opposite, adiabatic regime. Specifically, we take  $\omega_0/t = 0.1$  and  $\lambda = 0.25$ .

To quantify the effect of  $U$ , we show in Fig. 4(a) the suppression of  $T_c$  as a function of  $U$ . Starting from  $T_c/t = 0.204(1)$  at  $U = 0$ ,  $T_c$  decreases by about 15 percent in the range  $U \in [0, 0.5t]$ . In principle, in the spirit of an effective Holstein model, we can try to capture this effect by a coupling  $\lambda_{\text{eff}} = \lambda - U/W$ . However, Fig. 4(b) reveals that for the parameters considered this overestimates the effect of the Hubbard repulsion because  $T_c$  at

a given  $\lambda_{\text{eff}}$  in the Holstein model ( $U = 0$ ) is significantly lower than in the Holstein-Hubbard model ( $U > 0$ ). We attribute this finding to (i) the stronger suppression of the antiferromagnetic correlations (long-range magnetic order only exists at  $T = 0$ ) compared to the CDW correlations (CDW order exists also at  $T > 0$ ) at the temperatures considered, and (ii) retardation effects. A DMFT analysis of the Holstein-Hubbard model revealed that  $T_c$  is suppressed with increasing  $U$  at weak electron-phonon coupling but initially enhanced at strong coupling. This behavior was explained in terms of a reduction of the bipolaron mass due to the onsite repulsion [29].

## B. Critical behavior

In the thermodynamic limit, the long-range CDW order at  $T < T_c$  spontaneously breaks the sublattice symmetry. The two possible CDW patterns (cf. Fig. 1) imply the same critical behavior as the 2D Ising model and hence critical exponents  $\beta = 1/8$  and  $\nu = 1$ . Here, we demonstrate consistency with Ising universality for  $\omega_0/t = 0.1$  and  $\lambda = 0.25$ .

As the order parameter, the charge structure factor (5) should obey the finite-size scaling relation [21]

$$S_c(\mathbf{Q})/L^2 = L^{-2\beta/\nu} f_S[L^{1/\nu}(T - T_c)/T_c]. \quad (7)$$

Therefore, plotting  $S_c(\mathbf{Q})L^{2\beta/\nu-2}$  as a function of  $L^{1/\nu}(T - T_c)/T_c$  should produce a collapse of the data onto the curve described by the scaling function  $f_S$ . The best collapse [54] over the interval  $[-1, 1]$  in Fig. 5(a) gives  $T_c/t = 0.195(1)$ , smaller than the value  $T_c/t = 0.204(1)$  (Fig. 4) determined from finite-size scaling.

A similar analysis can be carried out for the correlation ratio, which is expected to obey

$$R_c = f_R[L^{1/\nu}(T - T_c)/T_c], \quad (8)$$

involving only the correlation length exponent  $\nu$ . Hence, we expect a collapse onto  $f_R$  by plotting  $R_c$  as a func-

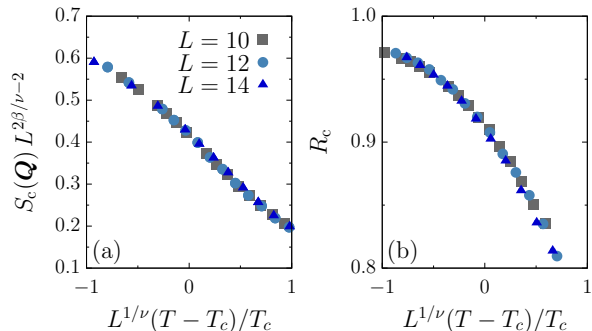


FIG. 5. Scaling collapse of (a) the structure factor and (b) the correlation ratio for  $\omega_0/t = 0.1$ ,  $\lambda = 0.25$ , and  $U = 0$  using the critical exponents of the 2D Ising model. The critical temperatures  $T_c$  were determined from the best scaling collapse and are given in the text.

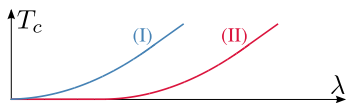


FIG. 6. The two possible scenarios for the phase diagram of the Holstein model. In scenario (I), we have CDW order with  $T_c > 0$  for any  $\lambda > 0$ . In scenario (II),  $T_c = 0$  for  $\lambda < \lambda_c(\omega_0)$ .

tion of  $L^{1/\nu}(T - T_c)/T_c$ . The best collapse on  $[-1, 1]$  is obtained for  $T_c/t = 0.205(1)$  and shown in Fig. 5(b). This critical value is consistent with the previous estimate  $T_c/t = 0.204(1)$  in Fig. 4. However, the collapse exhibits stronger scattering than for the structure factor, even though the correlation ratio is generally expected to be less affected by finite-size corrections [45].

### C. Phase diagram

Figure 1 gives the finite-temperature phase diagram of the Holstein model in terms of  $T_c(\lambda)$ , which separates the low-temperature phase with long-range CDW order from the high-temperature disordered phase. However, since accurate values of  $T_c$  at very small  $\lambda$  are currently not accessible, Fig. 1 does not settle the question of whether or not the ground state has CDW order for any  $\lambda > 0$ .

There are two well-understood limits. The *classical* Holstein model ( $\omega_0 = 0$ ) has a CDW ground state for any  $\lambda > 0$  and  $T_c > 0$  (see Sec. IV A). This follows from mean-field theory, which becomes exact at  $T = 0$ . In the opposite, antiadiabatic limit  $\omega_0 \rightarrow \infty$ , the Holstein model maps to the attractive Hubbard model, whose ground state has coexisting CDW and superconducting order but  $T_c = 0$ . Hence, as a function of  $\omega_0$ , the Holstein model interpolates between two limits that both exhibit long-range CDW order at  $T = 0$ .

Between these limiting cases (i.e., for  $0 < \omega_0 < \infty$ ), there appear to be two distinct scenarios for the shape of the phase boundary  $T_c(\lambda)$ , as illustrated in Fig. 6. In scenario (I),  $T_c > 0$  for any  $\lambda > 0$ , so that the ground state is always a CDW insulator. By contrast, in scenario (II),  $T_c = 0$  for  $\lambda < \lambda_c(\omega_0)$  and  $T_c > 0$  for  $\lambda > \lambda_c(\omega_0)$ . Case (II) can further be divided into (IIa) where CDW order exists at  $T = 0$  for any  $\lambda$ , and (IIb) with a disordered phase at  $T = 0$  below  $\lambda_c(\omega_0)$ . In scenario (I), the adiabatic (classical) fixed point determines the behavior for any finite  $\omega_0$ . On the other hand, in scenario (IIa), the physics is determined by the antiadiabatic fixed point for  $\lambda < \lambda_c(\omega_0)$  and by the adiabatic fixed point for  $\lambda > \lambda_c(\omega_0)$ . Note that CDW order with  $T_c = 0$  requires an emergent continuous order parameter, as realized for the attractive Hubbard model ( $\omega_0 = \infty$ ). However, the corresponding symmetry is broken for  $\omega_0 < \infty$  by retardation effects in the Holstein model [53].

A CDW ground state for any  $\lambda > 0$  may be expected based on the instability of the Fermi liquid. For the half-filled square lattice with nearest-neighbor hopping, the

noninteracting charge susceptibility  $\chi_c^{(0)}(\mathbf{Q}) \sim \ln^2 \beta t$  due to the combined effect of nesting and Van Hove singularities [16, 17]. In the Hubbard model, such divergences underlie the existence of an antiferromagnetic Mott insulator for any  $U > 0$ , and coexisting CDW and superconducting order for any  $U < 0$  [34]. For the Holstein model that does not have a symmetry-imposed degeneracy of CDW and pairing correlations, superconducting correlations were found to be weaker than CDW correlations at half-filling [17], consistent with the weaker divergence of the  $\mathbf{Q} = 0$  pairing susceptibility  $\chi_p^{(0)}(\mathbf{Q}) \sim \ln \beta t$ .

Despite these theoretical arguments, metallic and superconducting ground states were recently suggested for the half-filled Holstein and Holstein-Hubbard models based on variational QMC simulations [14, 15]. A metallic phase is also found within DMFT [55–57], where a Van Hove singularity is absent. For  $\omega_0 \ll t$ , the results of Fig. 1 appear consistent with CDW order even at  $T = 0$  for any  $\lambda > 0$ . On the other hand, the phase boundary  $T_c(\lambda)$  in Fig. 1 undergoes an increasingly strong shift to larger  $\lambda$  with increasing  $\omega_0$ , in principle compatible with  $T_c = 0$  at sufficiently weak coupling [scenario (II)]. In the significantly better understood 1D case, numerical results show that for  $\omega_0 > 0$  the ground state remains metallic for  $\lambda < \lambda_c$  despite a  $\ln \beta t$  nesting-related divergence of the charge susceptibility [12]. Since  $T_c = 0$  in the 1D case, this corresponds to scenario (IIb) above and is consistent with the  $\omega_0 = \infty$  limit, the 1D attractive Hubbard model. The latter has a metallic but spin-gapped Luther-Emery liquid [58] ground state and no long-range order. Functional renormalization group calculations for the 2D Holstein-Hubbard model exclude metallic or superconducting behavior at half-filling except for an extremely small region where  $T_c$  is essentially zero [31].

To address the ground-state phase diagram directly, we calculated the correlation ratios

$$R_c^x = 1 - \frac{\chi_c(\mathbf{Q} - \delta\mathbf{q})}{\chi_c(\mathbf{Q})}, \quad \mathbf{Q} = (\pi, \pi), \quad (9)$$

$$R_p^x = 1 - \frac{\chi_c(\mathbf{Q} - \delta\mathbf{q})}{\chi_c(\mathbf{Q})}, \quad \mathbf{Q} = (0, 0). \quad (10)$$

for CDW and s-wave pairing based on the susceptibilities

$$\chi_c(\mathbf{Q}) = \frac{1}{L^2} \sum_{ij} e^{i(\mathbf{r}_i - \mathbf{r}_j) \cdot \mathbf{Q}} \int_0^\beta d\tau \langle \hat{n}_i(\tau) \hat{n}_j \rangle, \quad (11)$$

$$\chi_p(\mathbf{Q}) = \frac{1}{L^2} \sum_{ij} e^{i(\mathbf{r}_i - \mathbf{r}_j) \cdot \mathbf{Q}} \int_0^\beta d\tau \langle \hat{\Delta}_i^\dagger(\tau) \hat{\Delta}_j \rangle, \quad (12)$$

where  $\hat{\Delta}_i = c_{i\uparrow} c_{i\downarrow}$ . The susceptibilities generally exhibit better finite-size scaling behavior than the corresponding static structure factors [cf. Eq. (5)]. We take a coupling  $\lambda = 0.075$ , for which Refs. [14, 15] suggest the absence of CDW order at  $U = 0$  over a large range of phonon frequencies. The inverse temperature was scaled as  $\beta t = 2L$  (with  $4 \leq L \leq 16$ ), which is at the current limit of the CT-INT method due to the sign problem.

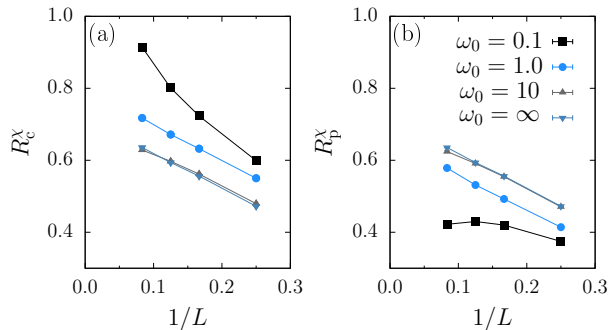


FIG. 7. (a) Charge and (b) pairing correlation ratios for different phonon frequencies. Here,  $\beta t = 2L$ ,  $\lambda = 0.075$ ,  $U = 0$ .

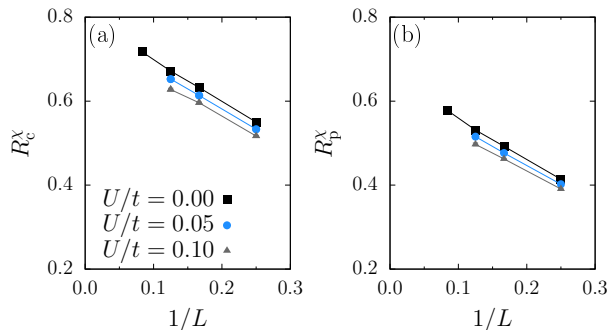


FIG. 8. (a) Charge and (b) pairing correlation ratios for different Hubbard repulsions. Here,  $\beta t = 2L$ ,  $\lambda = 0.075$ ,  $\omega_0/t = 1$ .

The correlation ratios shown in Figs. 7 and 8 have the same properties as discussed in Sec. IV A; long-range order is revealed by  $R_\alpha^x \rightarrow 1$  for  $L \rightarrow \infty$ , and a larger correlation ratio indicates stronger correlations in the corresponding channel. For  $\omega_0 = 0.1$ , the results in Fig. 7(a) suggest long-range CDW order, consistent with Fig. 1. At the same time, the pairing correlation ratio in Fig. 7(b) is strongly suppressed. Upon increasing  $\omega_0$ , CDW correlations are suppressed and pairing correlations enhanced, but  $R_c^x > R_p^x$  for any  $\omega_0 < \infty$ . Degenerate CDW and pairing correlations are only observed for the attractive Hubbard model ( $\omega_0 = \infty$ ). The fact that CDW correlations at  $\omega_0 < \infty$  are stronger than for  $\omega_0 = \infty$  suggests a CDW ground state also for the Holstein model and likely no superconducting order since  $T_c$  is already minimal for  $\omega_0 = \infty$ . As demonstrated in Fig. 8, a nonzero Hubbard repulsion suppresses both CDW and pairing correlations while enhancing antiferromagnetic correlations (not shown).

Figure 7 also reveals that in the weak-coupling regime where an absence of CDW order was predicted [14, 15], it is challenging to unequivocally detect the known  $T = 0$  long-range order of the attractive Hubbard model in terms of  $R_c^x, R_p^x \rightarrow 1$  for  $L \rightarrow \infty$ . The same should be true for the Holstein and Holstein-Hubbard model in the regime where  $T_c$  is small. Therefore, leaving aside the approximations inherent to variational QMC methods,

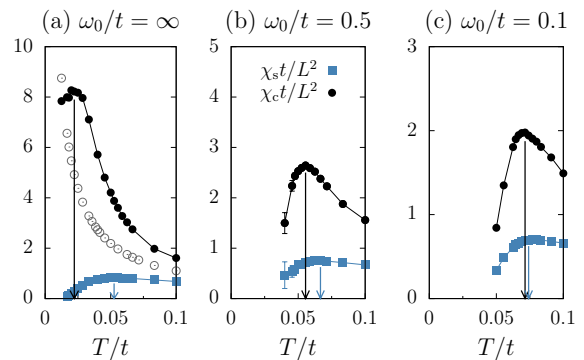


FIG. 9. Local spin and charge susceptibilities [Eq. (13)] for  $\lambda = 0.1$ ,  $U = 0$ , and  $L = 8$ . Open symbols in (a) are for  $\lambda = 0$ , arrows indicate maxima.

the reported absence of CDW order [14, 15] should also be taken with care.

While we are unable to provide a definitive  $T = 0$  phase diagram, the results of Fig. 7 together with the observation that long-range CDW order is known to exist at  $T = 0$  for both  $\omega_0 = 0$  and  $\omega_0 = \infty$  are consistent with CDW order but no superconductivity in the half-filled Holstein model at  $T = 0$ . Furthermore, in the absence of a higher symmetry relating CDW and superconducting order as in the attractive Hubbard model, we expect  $T_c > 0$  (although potentially exponentially small) and hence scenario (I) depicted in Fig. 6.

#### D. Bipolaron liquid

A final interesting point is the nature of the metallic phase at  $T > T_c$ . In the CDW phase, spin, charge, and hence also single-particle excitations are gapped. For 1D electron-phonon models, the spin gap persists in the metallic phase [12] and the  $T = 0$  CDW transition occurs at the two-particle level via the ordering of preformed pairs (singlet bipolarons) and the opening of a charge gap. The same is true for the 2D attractive Hubbard model for which the spin gap can be made arbitrarily large by increasing  $U$  while keeping  $T_c = 0$ . Hence, the disordered phase at low but finite temperatures is not a Fermi liquid but a metal with gapped single-particle and spin excitations [59, 60], the 2D analog of a Luther-Emery liquid [58]. Singlet bipolarons in principle also form for any  $\lambda > 0$  in the 2D Holstein model, although their binding energy ( $\sim \lambda$ ) can be small [61]. Nevertheless, we expect a spin-gapped metallic phase for suitable parameters. At sufficiently high temperatures, bipolarons undergo thermal dissociation [62].

To detect signatures of a spin-gapped metal, we consider the static charge and spin susceptibilities

$$\chi_c = \beta(\langle \hat{N}^2 \rangle - \langle \hat{N} \rangle^2), \quad \chi_s = \beta(\langle \hat{M}^2 \rangle - \langle \hat{M} \rangle^2) \quad (13)$$

with  $\hat{N} = \sum_i \hat{n}_i$ ,  $\hat{M} = \sum_i \hat{S}_i^x$ . Figure 9(a) shows results

for  $\lambda = 0.1$  and  $\omega_0/t = \infty$ . Whereas  $\chi_s/L^2$  diverges with decreasing temperature in a Fermi liquid (open symbols), it is strongly suppressed as  $T \rightarrow 0$  by the spin gap. The charge susceptibility is also suppressed at very low  $T$ , but  $\chi_c/L^2$  approaches a finite value determined by the density of  $T = 0$  charge fluctuations. The distinct temperature scales reflected by the maxima of  $\chi_s/L^2$  and  $\chi_c/L^2$  reveal the spin-gapped metallic phase at  $T > 0$  in the attractive Hubbard model. For the Holstein model,  $\chi_s/L^2$  is cut off by the spin gap, whereas  $\chi_c/L^2$  is cut off by the charge gap that appears at the CDW transition at  $T = T_c$ . The distinct maxima visible even in the adiabatic regime [Figs. 9(b) and 9(c)] are consistent with a spin-gapped phase at  $T > T_c$ . The extent of the latter appears to decrease with decreasing  $\omega_0/t$  and the phase is expected to be absent in the classical or mean-field limit ( $\omega_0 = 0$ ) where charge and spin gaps become equal. An immediate and important corollary of the existence of a spin-gapped metal of bipolarons above  $T_c$  would be that, contrary to expectations in previous work [24, 25], the appearance of a gap in the density of states does in general not imply CDW order. The additional spin-gap component is also compatible with experimentally observed large gap to  $T_c$  ratios [52].

In principle, a spin-gapped phase without long-range order (CDW or superconductivity) could also exist at  $T = 0$ , but the discussion in Sec. IV C provided arguments against a disordered phase. While well established in 1D electron-phonon models in terms of a Luther-Emery liquid [12], it would correspond to a so-called Bose metal [63] in higher dimensions. An interesting question

regarding the recent findings of Refs. [14, 15] is whether the variational wave functions used can distinguish between spin-gap formation and superconductivity. To this end, it would be useful to test this method for the intricate but well understood 1D Holstein model.

## V. CONCLUSIONS

We applied exact, continuous-time QMC simulations to the half-filled Holstein-Hubbard model on the square lattice. The critical temperature for the CDW transition was determined as a function of phonon frequency, electron-phonon coupling, and Hubbard repulsion from finite-size scaling. We also demonstrated the expected 2D Ising universality of this transition and addressed the ground-state phase diagram, providing data and theoretical arguments for the likely absence of a metallic or superconducting phase at weak coupling. Finally, we discussed the possibility of a spin-gapped metallic phase of bipolarons above  $T_c$ . The quantitative ground-state phase diagram remains an important open problem.

## ACKNOWLEDGMENTS

We thank F. Assaad, N. Costa, P. Bröcker, T. Lang, and R. Scalettar for helpful discussions and the DFG for support via SFB 1170 and FOR 1807. We gratefully acknowledge the computing time granted by the John von Neumann Institute for Computing (NIC) and provided on the supercomputer JURECA [64] at the Jülich Supercomputing Centre.

- 
- <sup>1</sup> P. A. Lee, N. Nagaosa, and X.-G. Wen, *Rev. Mod. Phys.* **78**, 17 (2006).  
<sup>2</sup> S. Manzeli, D. Ovchinnikov, D. Pasquier, O. V. Yazyev, and A. Kis, *Nat. Rev. Materials* **2**, 17033 (2017).  
<sup>3</sup> A. H. C. Neto, F. Guinea, N. M. R. Peres, K. S. Novoselov, and A. K. Geim, *Rev. Mod. Phys.* **81**, 109 (2009).  
<sup>4</sup> Y. Zhou, K. Kanoda, and T.-K. Ng, *Rev. Mod. Phys.* **89**, 025003 (2017).  
<sup>5</sup> T. Senthil, A. Vishwanath, L. Balents, S. Sachdev, and M. P. A. Fisher, *Science* **303**, 1490 (2004).  
<sup>6</sup> N. D. Mermin and H. Wagner, *Phys. Rev. Lett.* **17**, 1133 (1966).  
<sup>7</sup> S. Sorella, Y. Otsuka, and S. Yunoki, *Sci. Rep.* **2**, 992 (2012).  
<sup>8</sup> F. F. Assaad and I. F. Herbut, *Phys. Rev. X* **3**, 031010 (2013).  
<sup>9</sup> F. Parisen Toldin, M. Hohenadler, F. F. Assaad, and I. F. Herbut, *Phys. Rev. B* **91**, 165108 (2015).  
<sup>10</sup> Y. Otsuka, S. Yunoki, and S. Sorella, *Phys. Rev. X* **6**, 011029 (2016).  
<sup>11</sup> M. Hohenadler and T. C. Lang, in *Computational Many-Particle Physics* (Springer Berlin Heidelberg, 2008).  
<sup>12</sup> M. Hohenadler and H. Fehske, arXiv:1706.00470 (2017).  
<sup>13</sup> J. Greitemann, S. Hesselmann, S. Wessel, F. F. Assaad, and M. Hohenadler, *Phys. Rev. B* **92**, 245132 (2015).  
<sup>14</sup> T. Ohgoe and M. Imada, *Phys. Rev. Lett.* **119**, 197001 (2017).  
<sup>15</sup> S. Karakuzu, L. F. Tocchio, S. Sorella, and F. Becca, *Phys. Rev. B* **96**, 205145 (2017).  
<sup>16</sup> J. E. Hirsch and D. J. Scalapino, *Phys. Rev. Lett.* **56**, 2732 (1986).  
<sup>17</sup> F. Marsiglio, *Phys. Rev. B* **42**, 2416 (1990).  
<sup>18</sup> T. Holstein, *Annal. Phys.* **8**, 325 (1959).  
<sup>19</sup> R. T. Scalettar, N. E. Bickers, and D. J. Scalapino, *Phys. Rev. B* **40**, 197 (1989).  
<sup>20</sup> G. Levine and W. P. Su, *Phys. Rev. B* **42**, 4143 (1990).  
<sup>21</sup> R. M. Noack, D. J. Scalapino, and R. T. Scalettar, *Phys. Rev. Lett.* **66**, 778 (1991).  
<sup>22</sup> G. Levine and W. P. Su, *Phys. Rev. B* **43**, 10413 (1991).  
<sup>23</sup> M. Vekić, R. M. Noack, and S. R. White, *Phys. Rev. B* **46**, 271 (1992).  
<sup>24</sup> M. Vekić and S. R. White, *Phys. Rev. B* **48**, 7643 (1993).  
<sup>25</sup> P. Niyaz, J. E. Gubernatis, R. T. Scalettar, and C. Y. Fong, *Phys. Rev. B* **48**, 16011 (1993).  
<sup>26</sup> H. Zheng and S. Y. Zhu, *Phys. Rev. B* **55**, 3803 (1997).  
<sup>27</sup> J. E. Hirsch and S. Tang, *Phys. Rev. Lett.* **62**, 591 (1989).

- <sup>28</sup> E. Berger, P. Valášek, and W. von der Linden, *Phys. Rev. B* **52**, 4806 (1995).
- <sup>29</sup> J. K. Freericks and M. Jarrell, *Phys. Rev. Lett.* **75**, 2570 (1995).
- <sup>30</sup> C. Honerkamp, H. C. Fu, and D.-H. Lee, *Phys. Rev. B* **75**, 014503 (2007).
- <sup>31</sup> D. Wang, W.-S. Wang, and Q.-H. Wang, *Phys. Rev. B* **92**, 195102 (2015).
- <sup>32</sup> E. A. Nowadnick, S. Johnston, B. Moritz, R. T. Scalettar, and T. P. Devereaux, *Phys. Rev. Lett.* **109**, 246404 (2012).
- <sup>33</sup> S. Johnston, E. A. Nowadnick, Y. F. Kung, B. Moritz, R. T. Scalettar, and T. P. Devereaux, *Phys. Rev. B* **87**, 235133 (2013).
- <sup>34</sup> J. E. Hirsch, *Phys. Rev. B* **31**, 4403 (1985).
- <sup>35</sup> M. Hohenadler, F. F. Assaad, and H. Fehske, *Phys. Rev. Lett.* **109**, 116407 (2012).
- <sup>36</sup> M. Hohenadler and F. F. Assaad, *Phys. Rev. B* **87**, 075149 (2013).
- <sup>37</sup> M. Hohenadler, *Phys. Rev. Lett.* **117**, 206404 (2016).
- <sup>38</sup> A. N. Rubtsov, V. V. Savkin, and A. I. Lichtenstein, *Phys. Rev. B* **72**, 035122 (2005).
- <sup>39</sup> F. F. Assaad and T. C. Lang, *Phys. Rev. B* **76**, 035116 (2007).
- <sup>40</sup> E. Gull, A. J. Millis, A. I. Lichtenstein, A. N. Rubtsov, M. Troyer, and P. Werner, *Rev. Mod. Phys.* **83**, 349 (2011).
- <sup>41</sup> F. F. Assaad, “DMFT at 25: Infinite Dimensions: Lect. Notes of the Autumn School on Correlated Electrons,” (Verlag des Forschungszentrum Jülich, Jülich, 2014).
- <sup>42</sup> R. Blankenbecler, D. J. Scalapino, and R. L. Sugar, *Phys. Rev. D* **24**, 2278 (1981).
- <sup>43</sup> K. Michielsen and H. de Raedt, *Mod. Phys. Lett. B* **10**, 467 (1996).
- <sup>44</sup> K. Hukushima and K. Nemoto, *J. Phys. Soc. Jpn.* **65**, 1604 (1996).
- <sup>45</sup> K. Binder, *Z. Phys. B Con. Mat.* **43**, 119 (1981).
- <sup>46</sup> S.-J. Gu, *Int. J. Mod. Phys. B* **24**, 4371 (2010).
- <sup>47</sup> W.-L. You, Y.-W. Li, and S.-J. Gu, *Phys. Rev. E* **76**, 022101 (2007).
- <sup>48</sup> D. Schwandt, F. Alet, and S. Capponi, *Phys. Rev. Lett.* **103**, 170501 (2009).
- <sup>49</sup> A. F. Albuquerque, F. Alet, C. Sire, and S. Capponi, *Phys. Rev. B* **81**, 064418 (2010).
- <sup>50</sup> L. Wang, Y.-H. Liu, J. Imriška, P. N. Ma, and M. Troyer, *Phys. Rev. X* **5**, 031007 (2015).
- <sup>51</sup> M. Weber, F. F. Assaad, and M. Hohenadler, *Phys. Rev. B* **94**, 245138 (2016).
- <sup>52</sup> S. Blawid and A. J. Millis, *Phys. Rev. B* **63**, 115114 (2001).
- <sup>53</sup> J. E. Hirsch and E. Fradkin, *Phys. Rev. B* **27**, 4302 (1983).
- <sup>54</sup> O. Melchert, arXiv:0910.5403 (2009).
- <sup>55</sup> W. Koller, D. Meyer, Y. Ono, and A. Hewson, *Euro. Phys. Lett.* **66**, 559 (2004).
- <sup>56</sup> G. S. Jeon, T.-H. Park, J. H. Han, H. C. Lee, and H.-Y. Choi, *Phys. Rev. B* **70**, 125114 (2004).
- <sup>57</sup> Y. Murakami, P. Werner, N. Tsuji, and H. Aoki, *Phys. Rev. B* **88**, 125126 (2013).
- <sup>58</sup> A. Luther and V. J. Emery, *Phys. Rev. Lett.* **33**, 589 (1974).
- <sup>59</sup> R. R. dos Santos, *Phys. Rev. B* **50**, 635 (1994).
- <sup>60</sup> M. Randeria, N. Trivedi, A. Moreo, and R. T. Scalettar, *Phys. Rev. Lett.* **69**, 2001 (1992).
- <sup>61</sup> A. Macridin, G. A. Sawatzky, and M. Jarrell, *Phys. Rev. B* **69**, 245111 (2004).
- <sup>62</sup> M. Hohenadler and W. von der Linden, *Phys. Rev. B* **71**, 184309 (2005).
- <sup>63</sup> D. Das and S. Doniach, *Phys. Rev. B* **60**, 1261 (1999).
- <sup>64</sup> Jülich Supercomputing Centre, *J. Large-Scale Res. Facilities* **2**, A62 (2016).